

Numerical Study of Polytropes with $n = 1$ and Differential Rotation

T. L. Razinkova,^{1,*} A. V. Yudin,^{1,2,†} and S. I. Blinnikov^{1,3,‡}

¹*National Research Center Kurchatov Institute, Moscow, 123098 Russia*

²*Novosibirsk State University, Novosibirsk, 630090 Russia*

³*Kavli IPMU, Kashiwa, Chiba 277-8583, Japan*

The solution space of differentially rotating polytropes with $n = 1$ has been studied numerically. The existence of three different types of configurations: from spheroids to thick tori, hockey puck-like bodies and spheroids surrounded by a torus, separate from or merging with the central body has been proved. It has been shown that the last two types appear only at moderate degrees of rotation differentiability, $\sigma \simeq 2$. Rigid-body or weakly differential rotation, as well as strongly differential, have not led to any “exotic” types of configurations. Many calculated configurations have had extremely large values of parameter τ , which has raised the question of their stability with respect to fragmentation.

Keywords: stellar models, differential rotation, polytropes

I. INTRODUCTION

The study of rotating stars, or more generally self-gravitating bodies, has a long history, apparently dating back to Newton. The fundamental contributions to this field by such titans as Poincare and Chandrasekhar are well known [1]. However, its content can in no way be considered exhaustive: studies containing both analytical and numerical approaches to this problem are still regularly published.

Our study belongs to the second type, and here, we limited ourselves to considering a purely polytropic state equation with $n = 1$ (the adiabatic index is $\gamma = 2$). It should be noted that rotating polytropes with $n = 1$ attract special attention of theorists because the equilibrium equations in this case are linear (see Subsection II C below). In the literature, there are a sufficient number of (semi-)analytical solutions for this case (see, for example, [2, 3]) represented by infinite series in Legendre polynomials both for the case of rigid-body [4] and differential [5] rotations. The prefix “semi” means that, except in cases of weak rotation, the coefficients in the analytical expansions have to be found using one or another numerical method. To obtain

solutions, special techniques, for example, the introduction of oblate spheroidal coordinates were also used [6]. There were even studies [7] whose authors claimed to have found a *precise* analytical solution. However, subsequent criticism [8] demonstrated that this solution is only approximate.

A polytrope with $n = 1$ was considered as a model for studying the rotation of Jupiter-type planets and stars of type α -Eridani [9, 11, 12]. We are interested in this polytrope in the context of continuing research devoted to neutron stars [10]. In this research, we studied the evolution of low-mass neutron stars with rigid-body rotation. In this paper, we want to study the effects of rotation *differentiability* in the most general form. Although an accurate quantitative study of neutron stars is obviously only possible within the framework of the general theory of relativity, certain fundamental conclusions can be made while remaining within the framework of a purely Newtonian approximation. The polytrope with $n = 1$ in this context has another important property (see, for example, [13]): as is known, its radius (in the absence of rotation) is an eigenvalue of the problem and does not depend on the mass (or central density). Neutron stars in a wide range of masses have a similar property [14]: their radius changes very little and is of the order of 13 km [15].

The plan of this paper is as follows: in Section

* razinkova@itep.ru

† yudin@itep.ru

‡ blinnikov@bk.ru

II, the basic relations are given, the law of rotation is selected and a numerical method for constructing equilibrium stellar configurations is described. In Section III, the case of weakly differential rotation is analyzed. Section IV is the main section: it examines the case of $\sigma = 2$ in detail (see equation (9) below), and the main branches of solutions and structures of different types of calculated configurations are shown. In Section V, solutions for different with the aim of looking at the entire solution space as if “from above” and establishing relationships between different types (branches) of solutions are provided. In Section VI, the case $\sigma = 2$ is examined by one of the standard semi-analytical methods. There, we show that for moderately rotationally deformed configurations, the results of this approach coincide with our numerical solutions. However, it is impossible to describe highly compressed configurations with them. In conclusion, we summarize our findings and discuss prospects for further research.

II. BASIC DEFINITIONS, PARAMETERS, AND CALCULATION METHOD

We consider an axially-symmetric stellar configuration in a state of stationary rotation. The equilibrium equations are written in the form [1, 16]:

$$\frac{1}{\rho} \frac{\partial P}{\partial \xi} = - \frac{\partial \varphi_G}{\partial \xi} + \omega^2 \xi, \quad (1)$$

$$\frac{1}{\rho} \frac{\partial P}{\partial z} = - \frac{\partial \varphi_G}{\partial z}. \quad (2)$$

Here, P is the pressure, ρ is the density of the substance, φ_G is the gravitational potential, and ω is the angular velocity of rotation. Equation (1) describes the equilibrium of matter in a plane perpendicular to the axis of rotation, and $\xi = \sqrt{x^2 + y^2}$ is the cylindrical radius. In similar equation (2), z is the coordinate along the axis of rotation. We consider the case of a barotropic equation of state, i.e., $P = P(\rho)$. Then, introducing the enthalpy

$$H(\rho) \equiv \int \frac{dP'}{\rho'}, \quad (3)$$

and integrating equation (2), we obtain the Bernoulli integral:

$$H(\rho) + \varphi_G(\xi, z) = \Omega(\xi), \quad (4)$$

where $\Omega(\xi)$ is some function. Substituting this expression into (1), we obtain Poincare's theorem on the constancy of angular velocity on cylindrical surfaces coaxial to rotation, i.e. ω must be a function of only ξ , or $\omega = \omega(\xi)$. Hence, then follows the explicit form of function $\Omega(\xi)$ itself:

$$\Omega(\xi) = \int^\xi \omega(\xi')^2 \xi' d\xi' + \text{const.} \quad (5)$$

The equilibrium equation (4) together with expression (5) and the Poisson equation for the gravitational potential,

$$\Delta \varphi_G = 4\pi G \rho, \quad (6)$$

where Δ is the Laplace operator written for the considered case in cylindrical coordinates, forms the basis for solving the problem of a rotating axially symmetric star.

A. Code ROTAT

We briefly describe the algorithm implemented in the ROTAT program [17], which we use to find equilibrium rotating configurations of stars. It takes Bernoulli integral (4) as a basis and determines the density, which is substituted into the right-hand side of Poisson equation (6). The resulting equation contains only the gravitational potential. This equation is then written in finite differences on two-dimensional grid (r, ψ) , where r is the distance from the center of the configuration and ψ is the polar angle measured from the axis of rotation: $\xi = r \sin \psi$ and $z = r \cos \psi$. The grid is uniform in both coordinates. To calculate the area outside the sphere that covers the entire star, the following technique is used [18]: a replacement of $r \rightarrow 1/r$ is made and the equations are rewritten using this transformed variable. This allows calculations to be carried out in a finite region, and smooth stitching of

solutions is performed on the boundary of the sphere. At infinity, the condition of $\varphi_G \rightarrow 0$ is set. Fixing in addition to this the ratio of the polar and equatorial radii $\theta = R_p/R_e$ and maximal density makes it possible to determine field φ_G , and then all other quantities.

The coefficient matrix for the system of difference equations is sparse, i.e., it contains many zero elements. ROTAT uses a method for solving a system of linear equations (arising from the linearization of the full system in Newton's method) with sparse coefficient matrices that was described in [19]. The accuracy of the calculations is controlled by a virial test:

$$VT = \frac{1}{|W|} \left| 2T + W + 3 \int P dV \right|, \quad (7)$$

where T is the kinetic energy of the star's rotation, and W is its gravitational energy.

B. Law of Rotation

First, we define the law of rotation. It is well known (see, for example, [1]) that function $\omega(\xi)$ cannot be arbitrary: for rotation stability, the Zolberg–Heyland condition must be satisfied:

$$\frac{d\omega(\xi)\xi^2}{d\xi} \geq 0, \quad (8)$$

i.e., the angular momentum per unit mass cannot decrease during stationary stable rotation. This inequality motivated us to select from among all the possibilities the widely accepted law of rotation, which in our notation is written as follows:

$$\omega(\xi) = \frac{\omega_0}{1 + (\sigma-1) \frac{\xi^2}{R_e^2}}, \quad (9)$$

where ω_0 and σ are the constants. Parameter ω_0 automatically determined by the ROTAT code, once configuration compression θ is set. Parameter σ is set by the user and determines the degree of differential rotation: it shows how much faster the center rotates relative to the last point on the star's equator at $\xi = R_e$ ($\sigma = 1$ corresponds, naturally, to solid-body rotation). Taking into account constraint (8), rotation law (9) gives the potentially maximal possible degree of differentiability.

C. Equation of State

As was stated in the Introduction, the state equation was taken polytrope with $n = 1$. The equation of state is simply $P = K\rho^2$, where K is the constant, and the enthalpy is then equal to $H(\rho) = 2K\rho$. Linearity of dependence $H(\rho)$ leads to the fact that Bernoulli equation (4) also turns out to be a linear relation between density ρ and gravitational potential φ_G . Linearity of the relations between ρ and φ_G for $n = 1$ follows from the definition of polytropic index n [20]. This fact, along with the linearity of Poisson equation (6), makes it possible, generally speaking, to exclude ρ (or φ_G) in the explicit form, and obtain instead of a system of two equations for two functions a single equation (the Helmholtz equation) containing only one function.

The use of a polytropic equation of state also makes it possible all equations to be made dimensionless by introducing a characteristic length of $r_0 = \sqrt{K/2\pi G}$ and normalizing the density to its maximal value in the star ρ_m . The unit of mass in this case is $M_0 = 4\pi r_0^3 \rho_m$.

As is well known [13], in the absence of rotation (the spherically symmetric case), for a polytrope with $n = 1$, there is an explicit solution: $\rho = \rho_m \sin(x)/x$. The radius of a polytrope in dimensionless coordinates is equal to $R_e = \pi$. It is easy to show that the dimensionless mass M_s is also equal π . Below, we will use exactly these dimensionless quantities everywhere.

III. WEAKLY DIFFERENTIAL ROTATION

We begin the description of the obtained results with the case of relatively small rotation differential parameter σ . Figure 1 shows the calculated dependences of dimensionless masses $M_s(\theta)$ (left) and radius $R_e(\theta)$ (right) for four σ values: from $\sigma = 1$ (solid body rotation) to $\sigma = 1.8$. Configurations related to different σ differ in both color and type of symbols. All series of configurations start, obviously, from the point of $M_s = R_e = \pi$ at $\theta = 1$ (no rotation) and reach

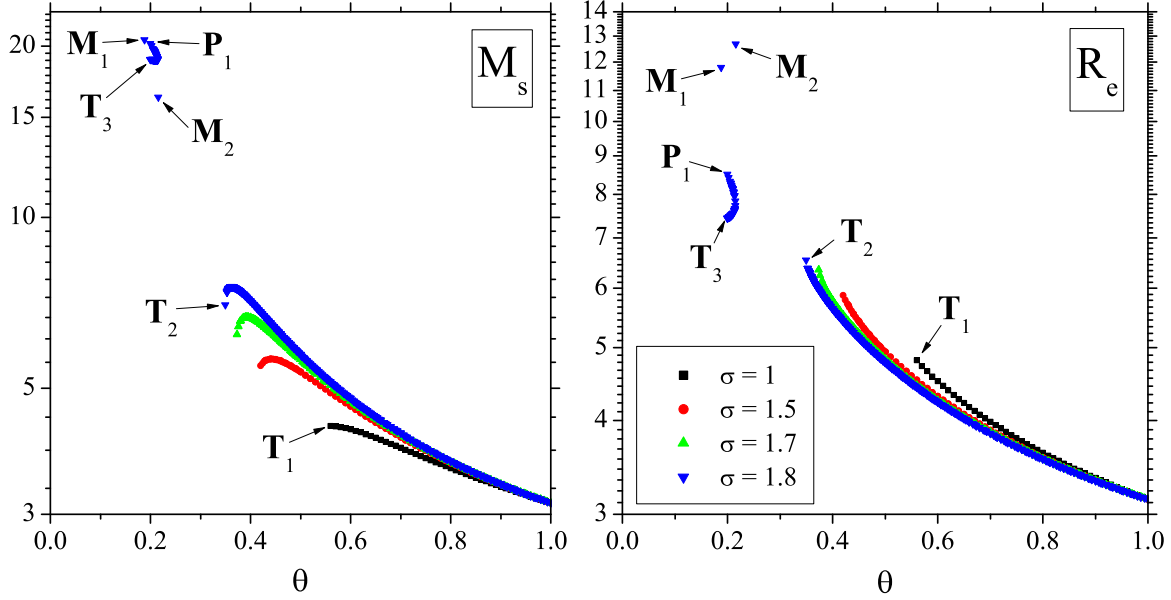


Рис. 1. Mass of a star M_s (left) and its equatorial radius R_e (right) as functions of parameter θ for several σ values. The arrows indicate the configurations whose structures are shown in the graphs below.

as σ grows to ever smaller θ values, where they break off.

Examples of the fastest rotating stars in these *continuous* series for the case of $\sigma = 1$ (configuration \mathbf{T}_1) and the case of $\sigma = 1.8$ (\mathbf{T}_2) are shown in Fig. 2. Here, the lines of the density level normalized to the maximum (see the color scale on the right) in coordinates in which the equatorial radius of the star is also normalized to unity, i.e., in coordinates $\{\xi/R_e, z/R_e\}$, are shown. Only a quarter of the entire configuration is shown: the star is symmetrical both relative to the abscissa axis (i.e., relative to the equatorial plane due to Lichtenstein's theorem, see, for example, [1]) and relative to the ordinate axis (the axis of rotation).

We return to Fig. 1. Obviously, as σ grows, the maximal flattening of the configurations increases, and this is exactly what should be expected. However, at $\sigma = 1.8$, something unexpected happens: after the gap of $0.216 \leq \theta \leq 0.35$, in which there are no solutions, two new types of configurations suddenly appear: \mathbf{P} and \mathbf{M} -type. They lie within the same narrow range of θ values, and here, the ambiguity (degeneracy) of the solution for this parameter

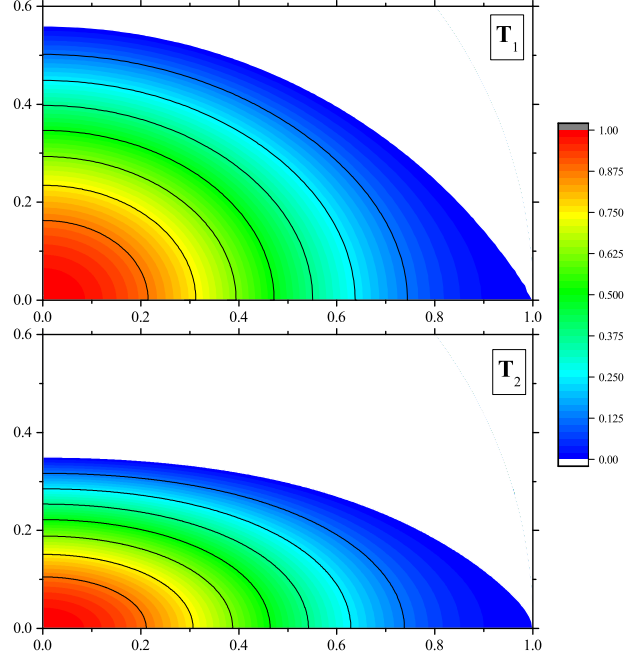


Рис. 2. Structure of configurations of \mathbf{T}_1 ($\sigma = 1$) and \mathbf{T}_2 ($\sigma = 1.8$) marked by arrows in Fig. 1 in normalized coordinates $\{\xi/R_e, z/R_e\}$. Details are in the text.

is manifested.

We first consider a series of configurations

that connect \mathbf{T}_3 and \mathbf{P}_1 . Its marginal structures are shown in Fig. 3. It is evident that, despite the

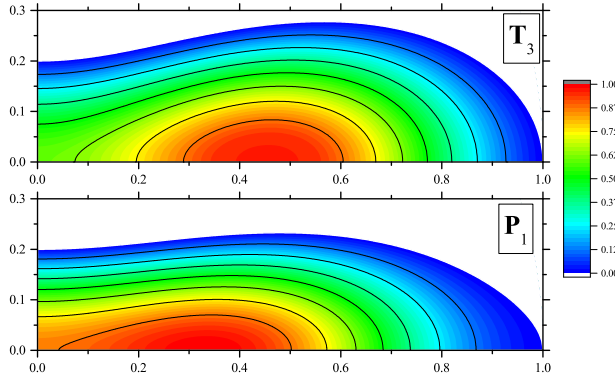


Рис. 3. Structure of configurations \mathbf{T}_3 and \mathbf{P}_1 (see Fig. 1).

almost identical flattening $\theta \approx 0.2$, configuration \mathbf{T}_3 is closer to the torus (hence, the name of this type), and \mathbf{P}_1 is more uniformly compressed and flat, resembling a hockey puck. It is interesting to note that these configurations (especially \mathbf{T}_3) resemble the “concave hamburger” obtained in [21]. We will see later that, generally speaking, configurations \mathbf{T} and \mathbf{P} are indeed separate and easily distinguishable types, but here, we observe their smooth transition into each other. The reason for this is discussed below in Section V.

Finally, we move on to an even more surprising type of configuration — type \mathbf{M} . Unlike types \mathbf{T} and \mathbf{P} , here, we do not even have a series, but only two solutions! Their structures are shown in Fig. 4. \mathbf{M}_1 is a structure similar to a matryoshka (russian doll) lying on its side (hence, the “M” is in the name of this type), and

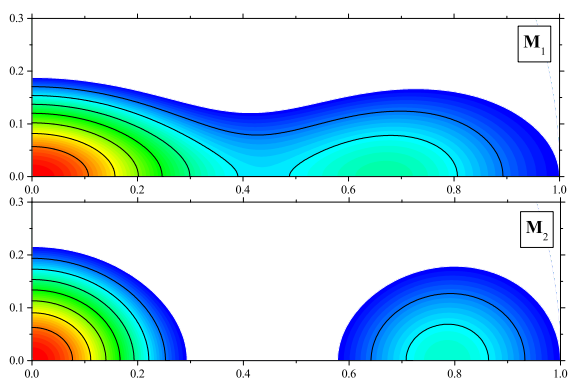


Рис. 4. Structure of configurations $\mathbf{M}_{1,2}$ (see Fig. 1).

\mathbf{M}_2 is a central body surrounded by a torus. It is interesting to note that configuration \mathbf{M}_2 is extremely similar to the spheroid-ring systems studied in [22], although for the case of solid-body rotation and incompressible fluid.

It is obvious that between \mathbf{M}_1 and \mathbf{M}_2 , it is possible to imagine a continuous transition, but despite all our tricks, we were unable to detect intermediate configurations. This may be due to the above-mentioned degeneration of solutions with respect to parameter θ : all intermediate solutions are “occupied” with a series from \mathbf{T}_3 to \mathbf{P}_1 .

IV. CASE $\sigma = 2$

We consider the option with $\sigma = 2$, i.e., the case when the center of the star rotates twice as fast as the last point of the star on the equator at $r = R_e$. This case is the most interesting since it not only contains all the types of rotating configurations we found, but is also characterized by a very non-trivial topology of curves in the space of the considered parameters. The latter are shown in Fig. 5.

The four panels of this figure show the following dependencies.

Top left: mass M_s as a function of the configuration compression parameter $\theta = R_p/R_e$.

Top right: equatorial radius $R_e(\theta)$.

Bottom left: $\tau(\theta)$, where $\tau \equiv E_{\text{rot}}/|W_g|$ is the dimensionless parameter equal to the ratio of the kinetic energy of rotation of a star E_{rot} to the modulus of its gravitational energy W_g . Quantity τ determines the importance of rotation effects and, in particular, is a critical indicator in the question of fragmentation of a rapidly rotating stellar configuration [1].

Bottom right: $\omega(\tau)$, where $\omega = J/I$ is the “average” angular velocity of rotation that is defined as the ratio of total angular momentum J of configuration to its inertia momentum I . For a rigid body rotating star, ω coincides with the angular velocity of rotation. Let us recall that all quantities considered here are dimensionless, in particular, is measured in units of $\sqrt{G\rho_m}$.

The colors indicate configurations that belong

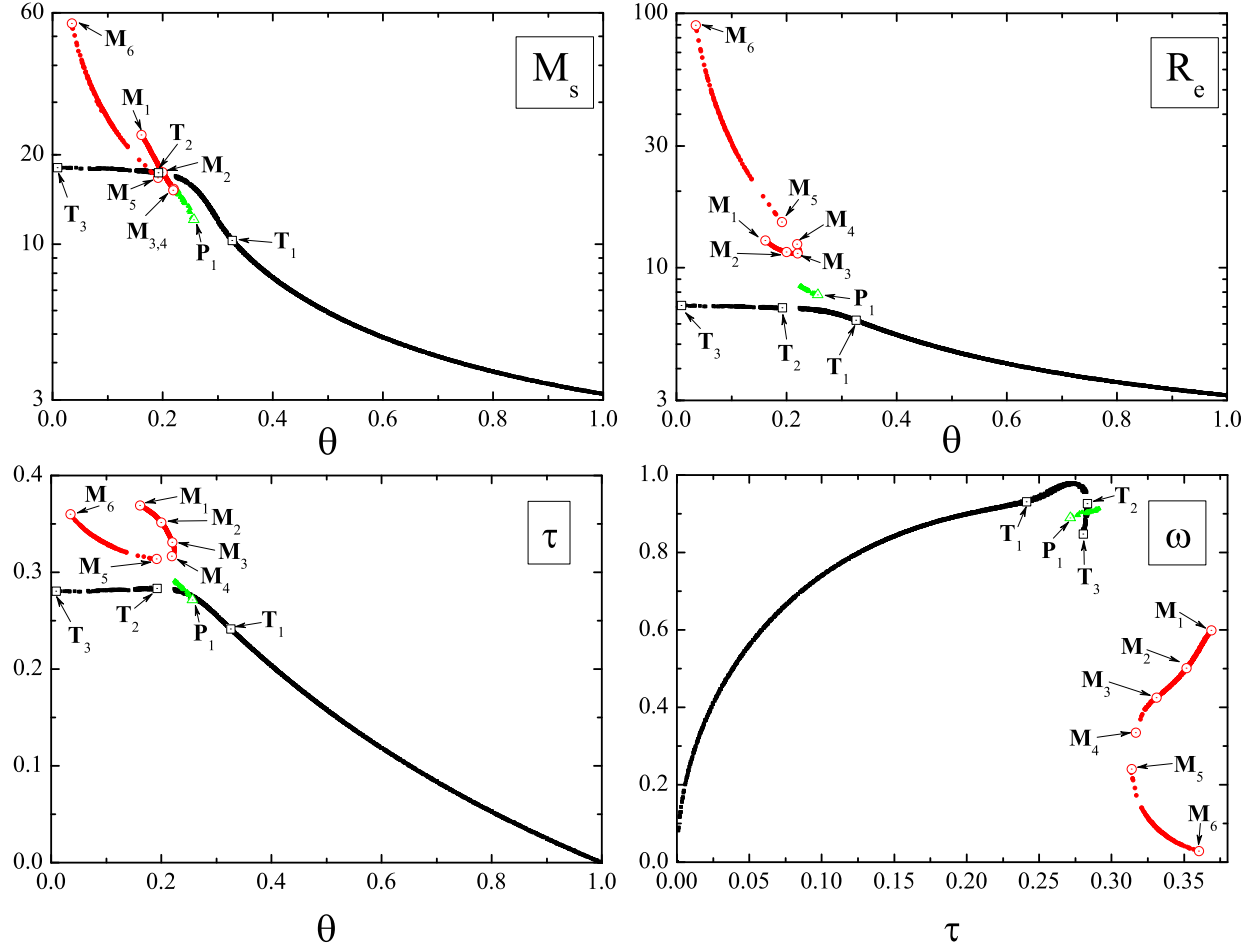


Рис. 5. Dependencies $M_s(\theta)$, $R_e(\theta)$, $\tau(\theta)$, and $\omega(\tau)$. Configurations of different types are highlighted in color. The large symbols with markings show the configurations shown below in Figs. 6, 7, and 8. Other details are in the text.

to different types. We begin our consideration with configurations of type **T** shown in black. They start with non-rotating configurations, for which $R_e = M_s = \pi$. At the same time, obviously, $\tau = \omega = 0$. As compression increases (θ decreases), all the considered parameters initially increase monotonically.

This continues until the value of $\theta \approx 0.25$, which is a bifurcation point: other types of configurations appear here, **P** and **M**, which we will describe later. It is interesting to note that the value of parameter τ is close in this case to the critical value $\tau \approx 0.27$ of the onset of dynamic instability with respect to fragmentation (see, for example, [1]). After that, growth of M_s , R_e and τ on the branch of **T**-type slows down significantly or stops completely, and

parameter ω , reaching its maximum with $\omega \approx 1$, begins to decrease.

What are configurations of type **T** and how do they change with the considered decrease in parameter θ ? The answer is given in Fig. 6. It shows the density level lines for configurations from **T**₁ to **T**₃ (see Fig. 5). Obviously, non-rotating configurations at $\theta = 1$ are spherically symmetric. Then, as the rotation rate increases, the configurations become increasingly flattened at the poles. Configuration **T**₁ shows a structure that is already sufficiently compressed and flat. It is also interesting to compare it with the structure of type **P** (see Fig. 7 and its discussion).

When moving towards **T**₂, an important phenomenon occurs: the place, where the density reaches its maximal value, shifts from the

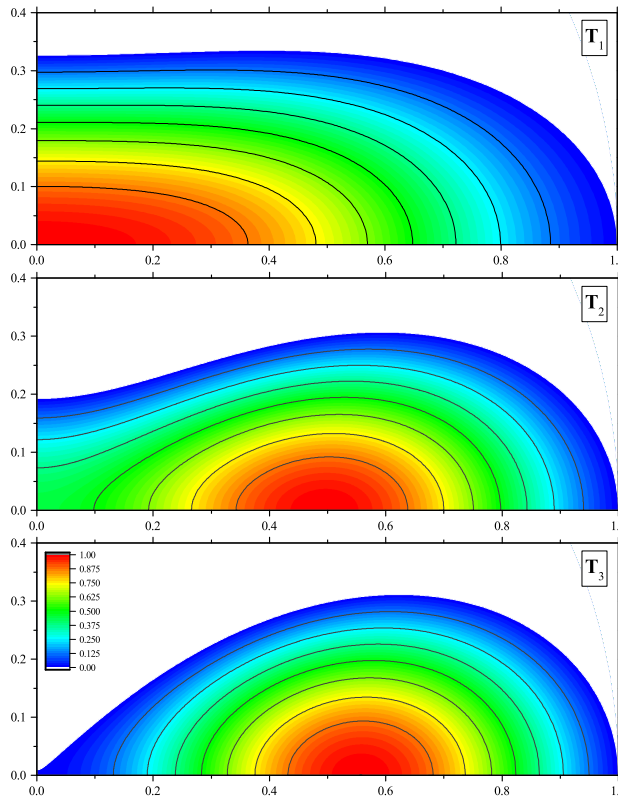


Рис. 6. Density level lines in configurations \mathbf{T}_1 – \mathbf{T}_3 (see Fig. 5)

center of the star to the periphery. The central region remains sufficiently “thick”. Ultimate configuration \mathbf{T}_3 corresponding to the value of $\theta = 0$ is a torus. It is important to note the difference between this torus and those toroidal structures described in the literature (see, for example, [23, 24]): it is thick, i.e., the main radius R of the torus comparable to its minor radius r . It is worth mentioning here that Wong worked with an incompressible fluid, while Ostriker, although considered, in particular, polytropes, used approximation $R \gg r$ everywhere.

We now consider configurations of other types that appear in calculations after bifurcation. We start with structures of type \mathbf{P} . They are shown in green in Fig. 5. As can be seen, they occupy a very small area of parameters in all diagrams, which is why in Fig. 7 we show the structure of only one of them (they all are very similar). These structures resemble a \mathbf{T}_1 flattened one and a half times (see Fig. 6). Despite this similarity, an examination of the

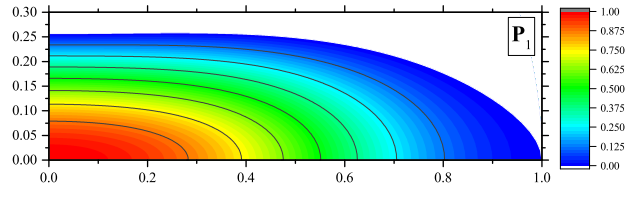


Рис. 7. Density level lines in configuration \mathbf{P}_1 (see Fig. 5).

various integral parameters shown in Fig. 5 shows that configurations of type \mathbf{P} represent a *separate* branch with its own unique properties.

We finally move on to the description of the extremely interesting branch with the \mathbf{M} marker (matryoshka doll). The reason for this, the name becomes clear from studying Fig. 8. We start with configuration \mathbf{M}_1 . It is something that vaguely resembles structures \mathbf{T}_1 or \mathbf{P}_1 , but with a more pronounced core and periphery separated by a noticeable deflection. Moving on through \mathbf{M}_2 to \mathbf{M}_3 , this deflection increases, and the section connecting the core with the periphery finally breaks during the transition to \mathbf{M}_4 . All subsequent configurations, including \mathbf{M}_4 , represent a central body surrounded by a torus. Moreover, when moving towards \mathbf{M}_6 the rotation becomes slower and slower, which is evident from the central part approaching spherical symmetry and the drop in parameter ω . The radius of the torus increases, making such configurations already significantly similar to those considered by Ostriker [23].

Despite its low density, this torus contains most of the mass of the system and significant angular momentum, as well as rotational energy, which is evident from the growth of parameter τ . It is important to note that *all* \mathbf{M} -configurations have extremely high values of $\tau > 0.3$, approaching in configurations \mathbf{M}_1 and \mathbf{M}_6 to the values of $\tau \simeq 0.36$. According to [25, 26], at this value, the rotating configuration becomes secularly unstable with respect to axially symmetric disturbances. It seems extremely interesting to study the stability of these structures, which, obviously, can only be done by performing a dynamic 3D-calculation. The authors are currently working on its implementation.

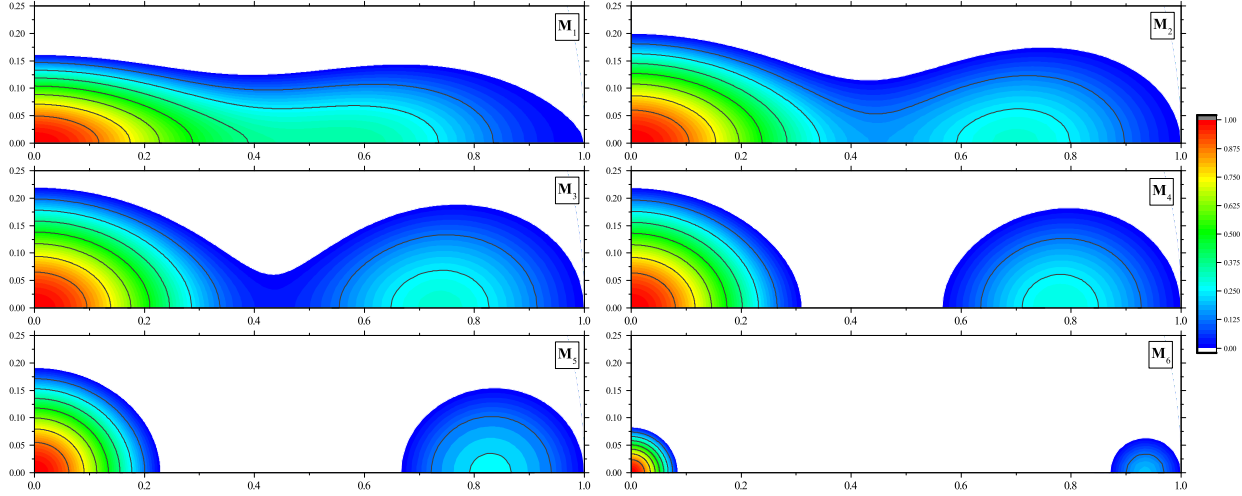


Рис. 8. Density level lines in configurations M_1 – M_6 (see Fig. 5).

Again, it is worth emphasizing that the structure of solutions turns out to be degenerate with respect to parameter θ : as can be seen in Fig. 5, different solutions may correspond to one θ value. On the other hand, it is noteworthy that in the range of values of another important parameter of $0.29 \lesssim \tau \lesssim 0.31$, there are no solutions at all.

V. GLOBAL DESCRIPTION

Despite the above-discussed case of relatively weak rotation and the special and most interesting case of $\sigma = 2$, the question about what happens globally with a gradual increase in parameter σ characterizing the degree of differential rotation still remains. What is needed here is, so to speak, a “top view” that would help to distract oneself from the particular characteristic of each specific value of σ and see the whole picture. This purpose, Fig. 9 shows the “Mass–Radius” diagram for several σ values.

We start with the area of small σ . In the lower left corner of the figure, the purple triangles show the case of $\sigma = 1.7$, which is also shown in Fig. 1. There are no “exotic” configurations here. They appear at $\sigma = 1.8$ (black squares) as a part of a “parabola” with branches upwards at $M_s \approx 20$ and $R_e \sim 7$ (it corresponds to configurations between \mathbf{T}_3 and \mathbf{P}_1 in Fig. 1) and in the form of two solutions of type \mathbf{M} falling on the branch

of “matryoshka” on the right ($M_s \gtrsim 15, R_e \gtrsim 11$). Already at $\sigma = 1.85$ (purple stars), the upper “parabola” splits into two branches. Thus, a small “parabola” at $\sigma = 1.8$ is the only bridge connecting types \mathbf{T} and \mathbf{P} .

It is interesting to follow the evolution of these branches as σ grows. The left branch of the parabola becomes more and more vertical and at $\sigma \sim 1.95 \div 2$ merges with the lower branch coming from non-rotating configurations, thus forming configurations of type \mathbf{T} . The right branch obviously goes into configurations of type \mathbf{P} , reaching its greatest prevalence at $\sigma = 1.95$ and gradually fading away to $\sigma = 2.1$.

Separately, it is necessary to consider the branch of configurations of type \mathbf{M} . It is most fully represented by the case of $\sigma = 2$. It is worth noting that the right side of the branch of \mathbf{M} -configurations extend far to the right and up beyond the area of the figure and is not shown simply to save space: such configurations represent a slowly rotating central body surrounded by a torus that is increasingly distant from it (see configuration \mathbf{M}_6 in Fig. 8). It is interesting that \mathbf{M} -configurations for all σ lie practically on the same branch, although there is no point in considering completeness or continuity in the sequence of configurations with different σ : taken separately, \mathbf{M} -solutions for $\sigma \neq 2$ represent, at first glance, a disparate set of points.

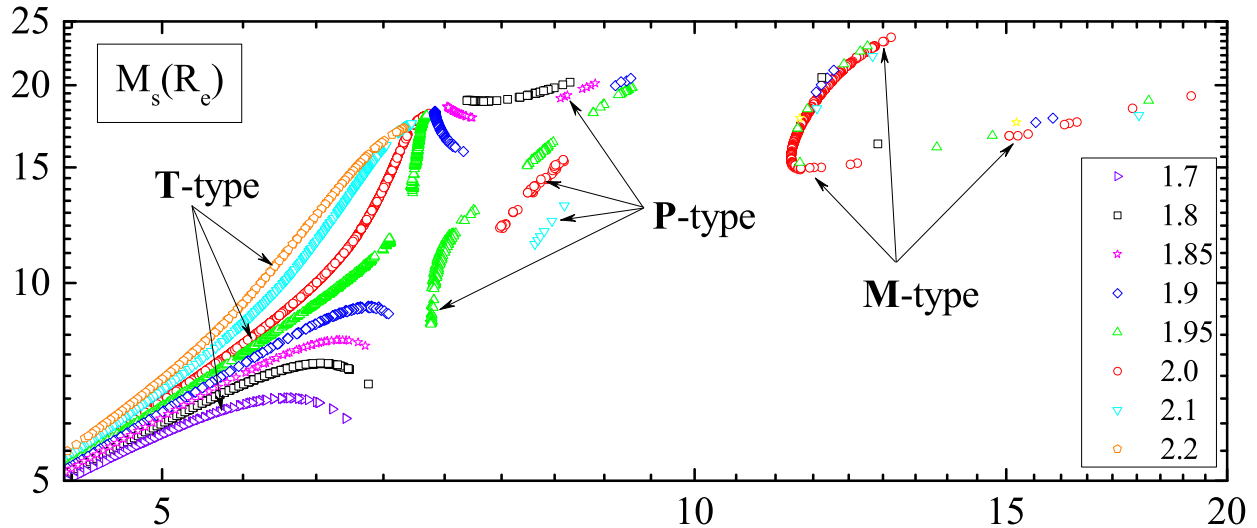


Рис. 9. Diagram $M_s - R_e$ for several values of parameter σ .

It should also be noted that at further growth of σ , no other “exotic” configurations arise, and the entire sequence of solutions for this σ represents one branch leading from non-rotating to T-configurations.

It is appropriate here to discuss the completeness of the presented solutions. In many branches in Fig. 9, breaks are visible, and M-solutions, as was already mentioned above, are often presented only as individual, single configurations. In our opinion, this seems to be a consequence of the already mentioned degeneracy of solutions with respect to input parameters, in particular, with respect to θ . The Newton iteration algorithm implemented in the ROTAT code in this case begins to “jump” between solutions, demonstrating poor convergence or lack thereof. Therefore, we cannot be absolutely sure of the completeness of the presented solutions. However, we can be sure of their *reality*. In fact, we managed using the well-known astrophysical code FLASH [27] to carry out 3D modeling of some of the above-considered “exotic” configurations of different types with extreme values of parameters, such as θ and τ . And all of them demonstrate hydrodynamic stability for at least tens of revolutions. This indicates that the hydrostatic equations for the initial configurations were solved correctly by the ROTAT code. The authors plan to publish the

results of this study in the near future.

VI. ANALYTICAL APPROACH

In light of some unusualness of some of the above results, their independent verification seems necessary. Below, we show the results of a standard analytical approach dating back to Chandrasekhar [28].

After the transition to dimensionless variables, the system of equations consisting of equilibrium equation (4) and Poisson equation (6) looks as follows:

$$\rho + \varphi = \Omega(\xi), \quad (10)$$

$$\Delta\varphi = \rho. \quad (11)$$

Due to the already noted linearity of the equations, this system is equivalent to one Helmholtz-type equation with respect to one of variables: ρ or φ .

In the case of relatively weak rotation, when the configuration of the star does not differ much from spherical, it seems natural to look for a solution in (r, μ) coordinates (where $\mu = \cos \psi$, see Fig. 10) in the form of an expansion in Legendre polynomials $P_k(\mu)$. The Laplace operator in this case is:

$$\Delta\varphi = \frac{1}{r^2} \frac{\partial}{\partial r} \left(r^2 \frac{\partial \varphi}{\partial r} \right) + \frac{1}{r^2} \frac{\partial}{\partial \mu} \left((1 - \mu^2) \frac{\partial \varphi}{\partial \mu} \right). \quad (12)$$

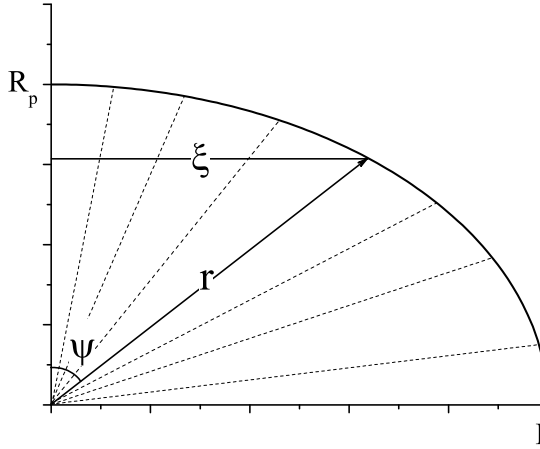


Рис. 10. Схематичное представление о computational domain and the boundary of the star.

Arbitrary function $f = f(r, \mu)$ can be expanded in a row:

$$f(r, \mu) = \sum_{k=0}^{\infty} f_{2k}(r) P_{2k}(\mu), \quad (13)$$

where it is taken into account that, due to the symmetry of the problem, the sum in (13) can contain only even indices. The orthogonality properties of Legendre polynomials make it possible to find explicitly functions $f_{2k}(r)$:

$$f_{2k}(r) = \frac{4k+1}{2} \int_{-1}^1 f(r, \mu) P_{2k}(\mu) d\mu \quad (14)$$

If we now express ρ from equation (10) and substitute it into (11), then, taking into account the properties of Legendre polynomials, we obtain the following equations for the components of the gravitational potential:

$$\varphi''_{2k} + \frac{2}{r} \varphi'_{2k} + \left[1 - \frac{2k(2k+1)}{r^2} \right] \varphi_{2k} = \Omega_{2k}(r), \quad (15)$$

where the primes denote derivatives with respect to r . The solution to the homogeneous equation is spherical Bessel functions $j_{2k}(r)$ and $y_{2k}(r)$, and, due to the limitations of φ at zero, only the first ones are suitable for us. We seek the solution of the inhomogeneous equation by the method of variation of constants, i.e., in the form of $\varphi_{2k} = c_{2k}(r) j_{2k}(r)$. Then, for c_{2k} , we obtain the equation:

$$(r^2 j_{2k}^2 c')' = r^2 \Omega_{2k} j_{2k}. \quad (16)$$

The solution to this equation is a double integral:

$$c_{2k} = \int \frac{dr_1}{r_1^2 j_{2k}^2(r_1)} \int r_2^2 \Omega_{2k}(r_2) j_{2k}(r_2) dr_2. \quad (17)$$

To simplify it, we use the following property of the Wronskian of the spherical Bessel functions [29]:

$$W(j_k(r), y_k(r)) = \begin{vmatrix} j_k & y_k \\ j'_k & y'_k \end{vmatrix} = \frac{1}{r^2}. \quad (18)$$

With its help, expression (17) can be reduced to a single integral, and the sought components of gravitational potential will $\varphi_{2k} = c_{2k} j_{2k}$ be written in the form:

$$\varphi_{2k}(r) = \int_0^r r_1^2 \Omega_{2k}(r_1) [y_{2k}(r_1) j_{2k}(r_1) - y_{2k}(r_1) j_{2k}(r)] dr_1 + C_{2k} j_{2k}(r), \quad (19)$$

where C_{2k} are some constants. From the condition of normalization at zero: $\rho(0) = 1$ and the fact that $\Omega(0) = 0$, we obtain that $C_0 = -1$.

A. External Solution and Stitching of Solutions

It is well known that the solution of the Poisson equation in a vacuum, regular at infinity, has an explicit solution for components (13) of the potential:

$$\varphi_{2k}(r) = A_0 \delta_{k0} + \frac{B_{2k}}{r^{2k+1}}, \quad (20)$$

where δ_{k0} is the Kronecker symbol, and B_{2k} are the constants.

At the edge of the star, density ρ turns to zero. Besides, potential φ and its gradient are continuous. The problem is that the shape of this boundary is not known in advance. We consider a method for numerically solving this problem (see, for example, [2]).

Let the angular velocity of rotation $\omega(\xi)$, and therefore, potential Ω be known. We restrict ourselves in expansions (13) to the N order, i.e., $k = (0 \div N)$. For internal potential (17), hereinafter designated by the index in, there is

N unknown coefficients C_{2k} because $C_0 = -1$ is specified. For the external (index (индекс out)) number of unknowns is $N + 2$ (A_0 and $N + 1$ of coefficients B_{2k}). We select $N + 1$ directions set by angles μ_i , as is shown in Fig. (10) by dashed lines. Then, we will have $N + 1$ unknown coordinates r_i of the star's surface corresponding to their angle μ_i . In total, we obtain the following $3(N + 1)$ unknowns. Each of $N + 1$ directions produces three equations:

$$\varphi^{\text{in}}(r_i, \mu_i) = \sum_{k=0}^N \varphi_{2k}^{\text{in}}(r_i) P_{2k}(\mu_i) = \Omega(\xi_i), \quad (21)$$

$$\varphi^{\text{out}}(r_i, \mu_i) = \sum_{k=0}^N \varphi_{2k}^{\text{out}}(r_i) P_{2k}(\mu_i) = \Omega(\xi_i), \quad (22)$$

$$\frac{d}{dr} \varphi^{\text{in}}(r, \mu_i) \Big|_{r=r_i} = \frac{d}{dr} \varphi^{\text{out}}(r, \mu_i) \Big|_{r=r_i}, \quad (23)$$

where, obviously, $\xi_i = r_i \sqrt{1 - \mu_i^2}$.

To calculate the derivative of quantities φ_{2k}^{in} , the properties of Bessel functions should be used: $f'_n = f_{n-1} - (n+1)f_n/x$ and $f'_0 = -f_1$, where $f = j$ or $f = y$.

B. Results of This Approach

We illustrate the results of the numerical approach described above using the example of the case of $\sigma = 2$. Figure 11 shows mass M_s of a star (left) and its equatorial radius R_e (right) as functions of θ .

Empty circles show calculations using the ROTAT program. Lines of different colors and types show calculations according to the algorithm described above for several values of N_{dir} , numbers of basic directions, namely, $N_{\text{dir}} = 2, 3, 4, 5, 7, 10$. For each N_{dir} , the angle distribution of directions is uniform.

The simplest case of $N_{\text{dir}} = 2$ (namely, the directions to the pole and the equator), as can be seen, is accurate only up to $\theta \gtrsim 0.85$. At lower θ , it systematically and greatly overstates the value of mass, which is simply taken B_0 with the opposite sign (see formula 20). Other values N_{dir} reproduce the parameters of stars much more accurately, and, obviously, the greater N_{dir} , the better. However, they all face a certain

peculiarity: when the value θ little less than 0.6, a numerical instability arises, which either leads to a “jump” to another solution (see, for example, the curves for $N_{\text{dir}} = 4, 5$) or to significantly worse convergence of iterations. This property is also characteristic of the calculations we performed for other σ . In general, it is not surprising that the smaller the value θ we take, the worse the convergence, and the greater the number N_{dir} must be taken to obtain correct results.

Using this method, we were unable to reproduce highly compressed configurations with $\theta \lesssim 0.4$ (the so-called “exotic”). This is not surprising: the lack of convergence of expansions in spherical harmonics in the case of strongly deformed configurations is widely known (see, for example, [30, 31]). To analyze them, algorithms of a different type are needed.

VII. CONCLUSIONS

In this paper, we have undertaken a detailed numerical study of polytropes with $n = 1$ and differential rotation. It should be noted here that conventional (semi-)analytical methods are usually based on expansions in some small parameters and are not applicable to the case, where the rotation is strong. We have obtained configurations of various types, with different topologies, and often with extreme values of such parameters as compression θ or fragmentation parameter τ .

We have identified the existence of three different types of configurations. Firstly, it is type **T**: a branch of solutions from non-rotating, spherically symmetric stars, through increasingly flattened objects to thick tori with $\theta \simeq 0$. Secondly, it is a small branch of type **P**: puck-like configurations distantly related to type **T**. This becomes clear only when studying configurations with $\sigma \sim 1.8$ (see the topology of the solution space in $M_s - R_e$ coordinates in Fig. 9). And finally, type **M**: a branch with solid figures resembling a matryoshka doll, on one side, and a quasi-spherical body surrounded by a torus, on the other side. It must be said that initially, we considered these two types of configurations

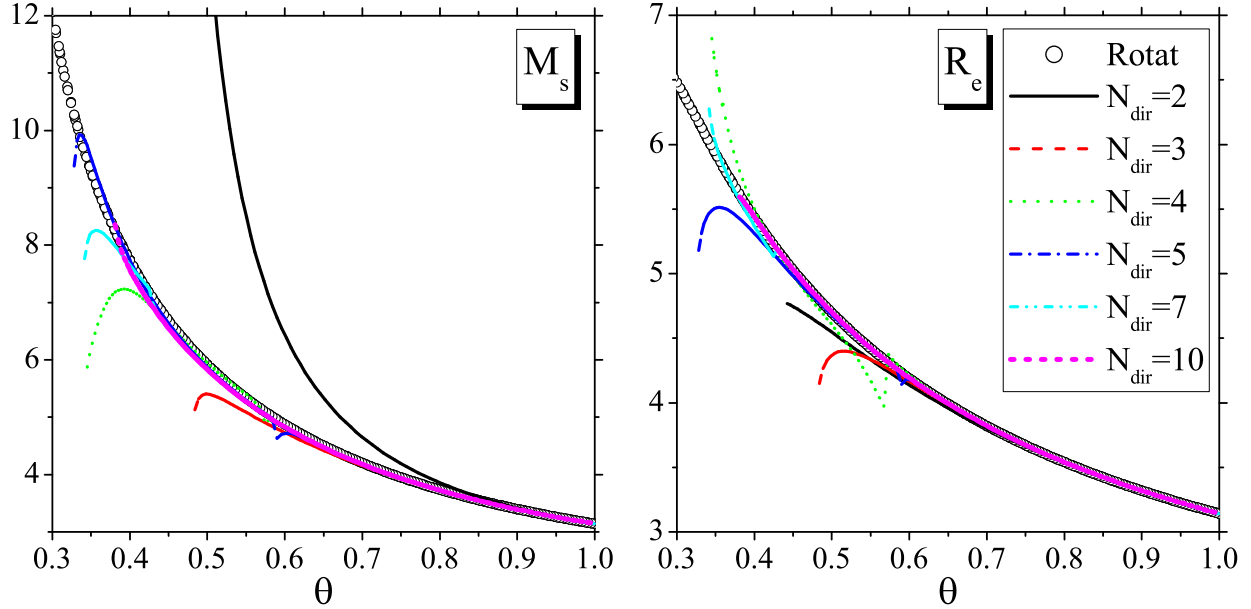


FIG. 11. Comparison of results of numerical approaches for $\sigma = 2$. On the left is the mass M_s of the star, and on the right is the equatorial radius R_e . Other details are in the text.

to be different, and only a huge number of calculations, especially for $\sigma = 2$, made it possible to find transitional forms and combine them into one branch.

An important finding is the conclusion that both weak differential rotation (with $\sigma \leq 1.7$) and strongly differential ($\sigma \geq 2.2$) do not lead to “interesting” configurations: here, all solutions lie on the branch connecting spheres with tori. All the “exotics” (configurations of types **P** and **M**) lie in the vicinity of $\sigma \sim 2$.

Finally, we discuss what still needs to be done in this area. To do this, we again refer to Fig. 5. The first question concerns configurations of type **M** that all have large values of parameter τ , whether they are fragile to fragmentation and if so, what type of fragmentation they undergo. We recall that after the loss of axial symmetry, the development of different types of instability is possible, in particular the so-called bar mode or ring mode [32]. In the first case, the rotating body is stretched along an axis perpendicular to the angular velocity vector and takes the form of a bar (cigar) rotating almost as a solid. In the second case, a ring is formed (for type **M**, it already exists), which then breaks up into several separate pieces.

Besides, the it is noteworthy configurations

of types **T** and **P** lying near the critical value of $\tau \simeq 0.27$, are they sustainable? It should be noted that the exact criterion for fragmentation is currently unknown. In the literature, various recipes for determining the stability of a rotating self-gravitating configuration have been proposed (see, for example, [33, 34]). Obviously, the answers to these questions must be given through appropriate 3D modeling of the fragmentation process, which the authors are currently working on.

Separately, it is necessary to mention the need for theoretical understanding of the obtained results. It is necessary to answer not only numerically, but also analytically, a whole series of questions that arise when analyzing the obtained data. Here is a list that is far from complete: first, what exactly causes the difference between configurations of types **T** and **P**, especially in areas where their parameters are close?

Second, how to describe configurations of type **M**? This apparently requires a generalization of the Ostriker’s study [23], which applies only to thin tori with $R_e \gg 1$ that surrounds the central object (i.e., to configurations of type **M**₆ in Fig. 8).

Thirdly, in Fig. 9, it is clear that the branches

of type **T** corresponding to different σ , all end in the area with $M_s \simeq 18$ and $R_e \simeq 9$. What determines these particular values? In fact, this is a question about the structure of “limit” tori with $\theta \sim 0$ (see configuration **T**₃ in Fig. 6).

The main problem of the analytical approach is that the application of standard methods dating back to Chandrasekhar [28, 35] based on expansions in terms of a small parameter (as a rule, this is the ratio of the characteristic hydrodynamic time of the problem and the rotation period, i.e., in order of magnitude ω) is impossible here: the rotation is strong, and the deviation of the configuration shape from spherical is very noticeable. In this regard, methods based on the use of so-called oblate spheroidal coordinates [6, 36] appear promising; their parameters are selected so that the density (enthalpy) isosurfaces are as close as possible to the coordinate isolines. Work within the framework of this approach is currently being carried out by the authors.

ACKNOWLEDGMENTS

The authors are grateful to the anonymous reviewer for valuable comments that greatly contributed to improving this article.

FUNDING

The work of A.V. Yudin was supported by the Russian Science Foundation, grant no. 22-12-00103.

CONFLICT OF INTEREST

The authors of this work declare that they have no conflicts of interest.

[1] J.-L. Tassoul, *Stellar Rotation: Theory of Rotating Stars* (Princeton Univ. Press, Princeton, NJ, 1979).

[2] V. V. Papoyan, D. M. Sedrakyan, and E. V. Chubaryan, *Astrofizika* 3, 41 (1967).

[3] Williams P.S. *Astroph. and Sp. Sc.*, 143, 2, 349-358 (1988).

[4] James R.A. *The Astroph. J.* 140, 552 (1964).

[5] S. I. Blinnikov, *Sov. Astron.* 16, 534 (1972).

[6] Cunningham C.T., *The Astroph. J.*, 211, 568-578 (1977).

[7] Kong D., Zhang K., Schubert G., *MNRAS* 448, 456-463 (2015).

[8] Knopik J., Mach P., Odrzywolek A., *MNRAS*, 467, 4, 4965-4969 (2017).

[9] Hubbard W.B., *Astron. Zh.*, 51, 1052-1059 (1975).

[10] A. V. Yudin, T. L. Razinkova, and S. I. Blinnikov, *Astron. Lett.* 45, 847 (2019).

[11] Kong D., Zhang K., Schubert G., Anderson J., *The Astroph. J.*, 763:116, 10 (2013).

[12] Vavruk M.V., Dzikovskiy D.V., *Contr. of Astron. Obs. Skalnate Pleso*, 50, 4, 748-771 (2020).

[13] Horedt G.P. *Polytropes: Applications in Astrophysics and Related Fields*, Kluwer Academic Publishers (2004).

[14] Haensel P., Potekhin A.Y., and Yakovlev D.G. *Neutron Stars 1 (Equation of State and Structure)* Springer, 619 (2007).

[15] Dittmann A.J. et al., arXiv:2406.14467 (2024).

[16] V. A. Krat, Figures of Equilibrium of Celestial Bodies (Gos. Izdat. Tekh.-Teor. Liter., Moscow, 1950) [in Russian].

[17] Aksenov A.G., Blinnikov S.I., *Astron. & Astrophys.*, **290**, 674-681 (1994).

[18] Clement M.J., *Astroph. J.*, **194**, 709-714 (1974).

[19] O. Osterby and Z. Zlatev, *Direct Methods for Sparse Matrices* (Springer, Berlin, 1983).

[20] Binney J., Tremaine S., *Galactic Dynamics*, second edition, Princeton University Press (2008).

[21] Hachisu I., Eriguchi Y., Sugimoto D., *Prog. of Theor. Phys.*, 68, 1, (1982).

[22] Basillais B., Hure J.M., *MNRAS*, 487, 4504-4509 (2019).

[23] Ostriker J., *Astroph. J.*, 140, 1056 (1964).

[24] Wong C.-Y. *Astroph. J.*, 190, 675-694 (1974).

[25] Bardeen J.M. *Astroph. J.*, 167, 425-446 (1971).

[26] Bodenheimer P., Ostriker J.P. *Astroph. J.*, 180, 159-169 (1973).

[27] Fryxell B. et al. *Astroph. J. Sup.*, 131, 1, pp. 273-334 (2000).

[28] Chandrasekhar S., Lebovitz N.R. *Astrophys. J.*, 136, 1082-1104 (1962).

[29] Olver F.W.J., Olde Daalhuis A.B., Lozier D.W., Schneider B.I., Boisvert R.F., Clark C.W., Miller B.R., Saunders B.V., Cohl H.S., and McClain M.A. *Digital Library of Mathematical Functions*, <http://dlmf.nist.gov/>, Release 1.1.1 of 2021-03-15.

[30] Balmino G., *Cel. Mech. and Dyn. Astron.*, 60, 3, pp.331-364 (1994).

[31] Bevis, M. et al., *Rep. on Prog. in Phys.*, 87, 7, 31 pp. (2024).

[32] Machida M.N., Omukai K., Matsumoto T., Inutsuka S.-I., *The Astroph. J.*, 677:813-827 (2008)

[33] Christodoulou D.M., Shlosman I., Tohline J.E., *The Astroph. J.*, 443:551-562 (1995).

[34] Hachisu I., Tohline J.E., Eriguchi Y., *The Astroph. J.*, 323, 592-613 (1987).

[35] Chandrasekhar, S., *MNRAS*, 93, 390-406 (1993).

[36] I. V. Komarov, I. V. Ponomarev, and S. Yu. Slavyanov, *Spheroidal and Coulomb Spheroidal Functions* (Nauka, Moscow, 1976) [in Russian].